PCCP

PAPER

View Article Online
View Journal | View Issue

Cite this: *Phys. Chem. Chem. Phys.*, 2016, **18**, 17470

Examining the structural evolution of bicarbonate–water clusters: insights from photoelectron spectroscopy, basin-hopping structural search, and comparison with available IR spectral studies†

Hui Wen,[ab] Gao-Lei Hou,[b] Yi-Rong Liu,[a] Xue-Bin Wang*[b] and Wei Huang*[ac]

Received 6th March 2016,
Accepted 23rd May 2016

DOI: 10.1039/c6cp01542e

www.rsc.org/pccp

Bicarbonate plays a crucial biochemical role in the physiological pH buffering system and also has important atmospheric implications. In the current study, $HCO_3^-(H_2O)_n$ (n = 0–13) clusters were successfully produced *via* electrospray ionization of the corresponding bulk salt solution, and were characterized by negative ion photoelectron spectroscopy and theoretical calculations. Photoelectron spectra reveal that the electron binding energy monotonically increases with the cluster size up to n = 10 and remains largely the same after n > 10. The photo-detaching feature of the solute HCO_3^- itself, which dominates in the small clusters, diminishes with the increase of water coverage. Based on the charge distribution and molecular orbital analyses, the universal high electron binding energy tail that dominates in the larger clusters can be attributed to the ionization of water. Thus, the transition of ionization from the solute to the solvent at a size larger than n = 10 has been observed. Extensive theoretical structural search based on the basin-hopping unbiased method was carried out, and a plethora of low energy isomers have been obtained for each medium and large-sized cluster. By comparing the simulated photoelectron spectra and calculated electron binding energies with the experiments, as well as by comparing the simulated infrared spectra with previously reported IR spectra, the best fit structures and the structural evolutionary routes are presented. The nature of bicarbonate–water interactions is mainly electrostatic as implied by electron localization function (ELF) analysis.

I. Introduction

The bicarbonate anion (HCO_3^-), an intermediate form in the deprotonation of carbonic acid, is one of the most common negative ions in nature.[1,2] Dissolution of CO_2 in water in the pH range of 8–10 mainly generates HCO_3^-.[3] It can also be produced by human carbonic anhydrase II (HCA II),[4,5] which catalyzes the hydration of CO_2. Hence, it plays an important role in biological processes such as pH regulation and transepithelial transport by membrane transporters.[6]

The HCO_3^- ion has been relatively well studied in both crystalline forms and solutions through various experimental approaches, such as X-ray diffraction, Raman, and infrared spectroscopy.[7–14] The thermochemical properties of the gas phase HCO_3^- ion have been studied *via* collision-induced dissociation (CID) and proton transfer reactions.[8] Hierl and Paulson[9] reported the threshold energy of 3.8 eV for the CID of HCO_3^- to HO^- + CO_2 in a tandem mass spectrometer. Wang *et al.* reported the first photoelectron spectroscopy of HCO_3^- and determined the adiabatic electron detachment energy (ADE)

[a] *Laboratory of Atmospheric Physico-Chemistry, Anhui Institute of Optics & Fine Mechanics, Chinese Academy of Sciences, Hefei, Anhui 230031, China. E-mail: Huangwei6@ustc.edu.cn*
[b] *Physical Sciences Division, Pacific Northwest National Laboratory, P. O. Box 999, MS K8-88, Richland, Washington 99352, USA. E-mail: Xuebin.Wang@pnnl.gov*
[c] *School of Environmental Science & Optoelectronic Technology, University of Science and Technology of China, Hefei, Anhui 230026, China*

† Electronic supplementary information (ESI) available: Optimized structures and bond parameters of $HCO_3^-(H_2O)_2$ at different levels of theory (Table S1); top 12 occupied molecular orbital energies of $HCO_3^-(H_2O)_n$, n = 0–13 (Table S2); low-lying isomers and relative energies of $HCO_3^-(H_2O)_n$, n = 3–13 (Fig. S1–S11); the stick density of states (DOS) spectra of the low-lying isomers of $HCO_3^-(H_2O)_{1-6}$ (Fig. S12) and $HCO_3^-(H_2O)_{7-12}$ (Fig. S13); simulated NIPE spectra of $HCO_3^-(H_2O)_n$, n = 1–12 (Fig. S14–S16); simulated IR spectra and comparison with the experiments in the frequency range of 600–1800 cm^{-1} (Fig. S17–S21); simulated IR spectra in the OH stretching range (2600–3800 cm^{-1}) (Fig. S22–S24); the most probable structures of $HCO_3^-(H_2O)_n$ proposed in this work (Fig. S25); molecular orbitals of the minimum energy isomers (Fig. S26–S30); symbols and labels of each atom in $HCO_3^-(H_2O)_{10}$ (Fig. S31); top five low-lying isomers of $HCO_3^-(H_2O)_n$ (n = 9–13) in the 'ball' display format. See DOI: 10.1039/c6cp01542e

of HCO_3^- to be 3.680 ± 0.015 eV, which also represents the electron affinity (EA) of the $HCO_3^\bullet$ neutral radical.[10]

The HCO_3^- ion has often been employed as a benchmark to study the solvation effects on chemical reaction dynamics.[11–16] The structural and dynamical properties of the hydrated HCO_3^- ion are also of great significance for the detailed understanding of the chemical processes in aqueous bicarbonate salt solutions, in particular its role in biology and in the atmosphere.[3] Keesee *et al.* reported the equilibrium thermodynamic data on the first four hydrates of HCO_3^-, and they determined the hydration enthalpy of the HCO_3^- ion to be −95 kcal mol^{-1} in the gas phase by high-pressure mass spectrometry.[17] Rudolph *et al.* studied the vibrational spectra of dilute solutions of $KHCO_3$ and $KDCO_3$, and suggested that the hydrated HCO_3^- anion possesses C_1 symmetry, which is in contrast to the planar (C_s symmetry) structure expected in the gas phase.[18,19] Recently, Asmis and co-workers investigated microsolvated HCO_3^- anion–water clusters by studying stepwise hydration effects on spectroscopy, structures, and energetics using infrared multiple photon dissociation spectroscopy (IRMPD).[20]

Theoretically, Leung *et al.* employed *ab initio* molecular dynamics (AIMD) to simulate hydrated systems containing 63 water molecules and a solute (either CO_2, HCO_3^-, or OH^-). They found that HCO_3^- and CO_3^{2-} exhibit a great tendency to coordinate with water molecules, forming on average 6.9 and 8.7 hydrogen bonds, respectively.[15] The *ab initio* quantum mechanical charge field molecular dynamics (QMCF MD) formalism was applied to simulate the bicarbonate ion in aqueous solution by Rode *et al.*, and the difference in coordination numbers was obtained.[21] Recently, Car–Parrinello (CP) MD simulations have been performed for aqueous carbonate species, *i.e.*, H_2CO_3, HCO_3^-, CO_3^{2-} and CO_2, providing quantitative information with respect to hydrogen bond environments for these important species and their effects on the structure and dynamics of the surrounding water molecules.[16]

Despite the aforementioned experimental and theoretical studies of HCO_3^- in the gas phase, in solutions, and in its hydrated clusters, the significant roles of HCO_3^- in biological systems and in atmospheric chemistry as well as the complex hydration structures warrant a further spectroscopic study and detailed theoretical modeling to elucidate the chemical bonding and underlying solute–solvent interactions that determine energetics, structures, and dynamics of this important species in solutions and at interfaces. In this paper, we report a low-temperature negative ion photoelectron spectroscopy (NIPES) study of the $HCO_3^-(H_2O)_n$ (n = 0–13) hydrated clusters. The measured photoelectron spectra with the accompanying electronic structure calculations and wave function analyses provide a detailed probe for micro-solvation of HCO_3^-.

The highlights of this paper are as follows: (1) we presented the size-selected photoelectron spectra of $HCO_3^-(H_2O)_n$ clusters with up to 13 water molecules; (2) a more extensive theoretical structural search based on the basin-hopping unbiased method has been carried out; (3) a set of structures that best fit the experiments and are most likely to be the global minima of $HCO_3^-(H_2O)_n$ clusters are proposed; and (4) the interaction nature of hydrated bicarbonate was investigated by wave function analyses.

II. Experimental and theoretical methods

A. Experimental details

The NIPES experiments were carried out using a low-temperature PES apparatus coupled with an electrospray ionization source, the details of which has been described previously.[22] The desired $HCO_3^-(H_2O)_n$ (n = 0–13) cluster anions were produced *via* electrospraying ~10^{-4} molar solution of $NaHCO_3$ salt dissolved in a mixture of acetonitrile–water solvent (3/1 volume ratio). The produced anions were guided by two radio frequency quadrupole ion guides, directed by a 90° bender into a temperature controlled 3D Paul trap, where they were accumulated and collisionally cooled with 0.1 mTorr cold buffer gas (20% H_2 seeded in He) at 20 K for a period of 20–100 ms. Previous studies have demonstrated that very cold ions can be generated in this way.[22–26] After cooling in the trap, the cold ions were pulsed out into the extraction zone of a time-of-flight (TOF) mass spectrometer at a 10 Hz repetition rate for mass-to-charge ratio and size analysis.

For each NIPES experiment, the $HCO_3^-(H_2O)_n$ (n = 0–13) anions were first mass-selected and decelerated before being interacted with a 157 nm (7.867 eV) laser beam from a F_2 excimer laser in the photodetachment zone of a magnetic bottle photoelectron analyzer. The laser was operated at a 20 Hz repetition rate with the ion beam off at alternating laser shots for shot-to-shot background subtraction. Photoelectrons were collected at nearly 100% efficiency by the magnetic bottle and analyzed in a 5.2 m long electron flight tube. The TOF photoelectron spectra were collected and converted to kinetic energy spectra calibrated by the known spectra of I^- and $Cu(CN)_2^-$.[24] The electron binding energy (EBE) spectra presented in the paper were obtained by subtracting the kinetic energy spectra from the detachment photon energy. The electron energy resolution was about 2% (*i.e.*, 20 meV for 1 eV kinetic energy electrons).

B. Theoretical methods

The basin-hopping (BH) algorithms with metropolis sampling and local optimization techniques were employed to search the cluster structures. This method has been successfully employed to explore the structures of nano-clusters, especially for atomic clusters.[27–31] Recently, by modifying the searching program, we have shown that it is also useful for searching the structures of molecular clusters.[32]

We performed an extensive search for the energy minimum structures of $HCO_3^-(H_2O)_n$ (n = 0–13) clusters using the modified BH method coupled with density functional theory (DFT). To generate isomer populations in the initial BH search, the gradient-corrected Perdew–Burke–Ernzerhof (PBE)[33] exchange correlation functional and the double numerical polarized (DNP) basis set with effective core potentials (ECPs) as implemented in the DMol^3 code[34] were used with a medium level convergence criterion.

Hundreds of structures were sampled for each size of clusters, especially for the large size clusters. The isomers for each cluster were ranked according to their relative energies for further optimization at higher levels. The low-lying energy isomers in each case were further optimized using the Becke's three-parameter hybrid exchange functional with the Lee, Yang, and Parr (B3LYP) functional and the 6-311++G** basis set.[35] We also tested the three-parameter functional of Cohen and Handy (O3LYP),[36] the three-parameter functional of Xu and Goddard (X3LYP),[37] the hybrid functional of Truhlar and Zhao variation M06-2X,[38] as well as the exchange component of the Perdew and Wang's 1991 functional (PW91),[39] all implemented in the Gaussian 09 package.[40]

Single point energy calculations were performed at higher levels of theory, B3LYP, Møller-Plesset (MP2) and density-fitting local Møller-Plesset (DF-LMP2) methods with the Pople's all electron basis set 6-311++G(3df,3pd). Harmonic vibrational frequencies were calculated to confirm that the obtained isomers are the true minima. The MP2 and DF-LMP2 calculations were performed using Molpro 2010.1.[41,42] Theoretical vertical detachment energy (VDE) of each species is calculated as the energy difference between the anion and neutral, both at the optimized anion's geometry for each cluster. The final VDEs reported in this paper were obtained at the B3LYP/6-311++G(3df,3pd) level of theory. All relative energy calculations included zero-point-energy (ZPE) corrections.

III. Experimental results

Fig. 1 presents the 157 nm NIPE spectra of $HCO_3^-(H_2O)_n$ (n = 0–13) taken at an ion trap temperature of 20 K. Higher resolution spectra of the bare HCO_3^- at 266 and 193 nm have been reported previously,[10] showing a very broad feature spanning from 3.6 to 4.9 eV (X), followed by a sharp and intense peak A starting at EBE = 5.11 eV with a partially resolved vibrational progression. The rather weak and slow rising edge of band X is better-resolved and amplified at 266 nm, showing a partially resolved structure dominant with one vibrational mode of 530 ± 20 cm^{-1}.[10] Compared with the spectra taken at 266 and 193 nm, the 157 nm (Fig. 1) spectrum of HCO_3^- shows quite different shapes – the originally weak, slow rising edge of the X band becomes sharp and better resolved, and the intensity of X becomes intense, equal to that of band A. An extra band (B) exhibits at higher EBE region (5.8 eV–6.5 eV) with a clear band gap from the sharp and intense peak A. There is no other feature beyond 6.5 eV. No vibrational features are discernible for all bands at 157 nm.

The NIPE spectra of $HCO_3^-(H_2O)_n$ (n = 1–13) clusters are similar to that of the bare HCO_3^-, except that the EBEs increase systematically due to solvent stabilization. Since no vibrational structures are resolved in the 157 nm spectra, we cannot obtain accurate ADEs for the hydrated HCO_3^- clusters. To help evaluate the spectral shift due to solvent stabilization, we estimated the apparent threshold detachment energy (TDE) from the threshold onset point of the X band in each spectrum, and listed TDEs for all clusters in Table 1. The solvation stabilization can be vividly seen in dashed lines connected to those TDEs (Fig. 1). We observed a monotonic increase of TDEs from n = 0 to 10. It is notable that the spectra no longer shift to a higher EBE region after $n > 10$. It is also interesting to see that the photo-detaching feature of HCO_3^- itself diminishes with increase of water coverage, and almost invisible for the large clusters ($n > 10$). Instead, a

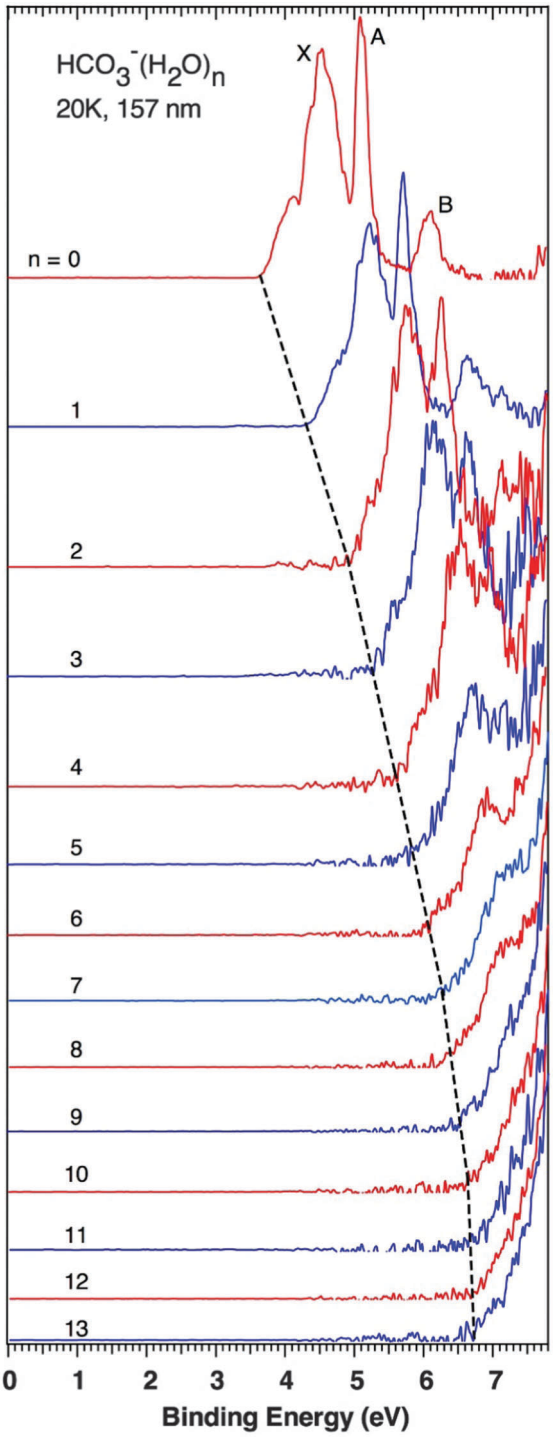

Fig. 1 The 20 K photoelectron spectra of $HCO_3^-(H_2O)_n$ (n = 0–13) at 157 nm (7.867 eV).

Table 1 Vertical detachment energies (VDEs, in eV) measured from the maximum of the first spectral features and calculated from the local minima of each $HCO_3^-(H_2O)_n$ (n = 0–13) clusters. The threshold detachment energy (TDE) estimated from each spectral threshold is also listed

n	Exp. VDEs[a]	Cal. VDEs[b]	TDE[a]
0	4.15(2)	4.10	3.60(2)
1	4.85(3)	4.84	4.31(3)
2	5.35(3)	5.30	4.83(3)
3	5.70(3)	5.64	5.20(3)
4	6.05(3)	6.02	5.58(3)
5	6.30(5)	6.20	5.76(3)
6	6.50(5)	6.31	6.03(3)
7	6.65(5)	6.40	6.19(3)
8	6.75(5)	6.49	6.32(3)
9	6.85(5)	6.58	6.50(3)
10	6.95(5)	6.55	6.62(3)
11	6.95(5)	6.61	6.62(3)
12	6.95(5)	6.64	6.62(3)
13	6.95(5)	6.68	6.62(3)

[a] Numbers in parentheses represent experimental uncertainties in the last digit. [b] Obtained at the B3LYP/6-311++G(3df,3pd) level of theory.

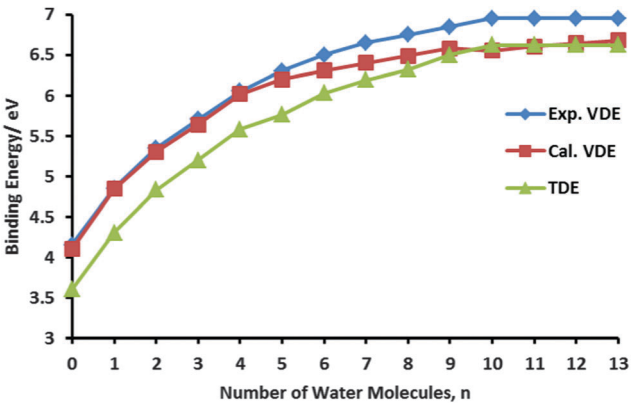

Fig. 2 Experimental and theoretical vertical detachment energy (VDE), as a function of number of water molecules, n. The threshold detachment energy TDE is also plotted for comparison.

featureless rising spectral tail starts to exhibit near the photon energy limit for the clusters $n > 3$ and becomes dominant for the large clusters $n > 9$. We suspect that this universal high EBE tail that dominates for the large clusters is due to the ionization of solvent water.[43] For each of those clusters, in which a spectral shoulder on the rising edge of the X band is visible, we could estimate the experimental VDE from the maximum of the partially resolved spectral shoulder. For other larger clusters, in which the spectral shoulders are no longer discernible in the X bands, we approximated their VDEs by adding the |VDE − TDE| difference averaged from the neighboring clusters to their corresponding TDEs. The VDEs estimated in this way for $HCO_3^-(H_2O)_n$, n = 0–13 clusters are summarized in Table 1 and presented in Fig. 2.

IV. Theoretical results and discussion

A. Theoretical results

In order to employ a suitable method to proceed with these clusters, we tested several DFT functionals, such as B3LYP, O3LYP, X3LYP, PW91, M06-2X, and M06-L together with the Pople basis set 6-311++G** to optimize the structures and compare with the results obtained by the higher level MP2 method. It is found that the bond lengths obtained with both the B3LYP and X3LYP functionals agree well with those obtained using the MP2 method, (refer to Table S1 in the ESI† for details). Therefore, we employed the B3LYP/6-311++G** level of theory to optimize all the structures studied in the current work. The typical low-lying isomers of the $HCO_3^-(H_2O)_n$ (n = 1–13) clusters are presented in Fig. 3 and 4. Complete lists of the low-lying isomers obtained in this study are available in Fig. S1–S11 in the ESI† of this manuscript.

The density of states (DOS) spectra of the minimum energy isomer and one selected low-lying isomer were calculated to compare with the experimental spectra based on the theoretically generalized Koopmans' theorem,[44] in which the observed spectral features can be viewed as originating from electron removal from specific occupied orbitals of the anion. The simulated spectra are obtained by setting the highest occupied molecular orbital (HOMO) transition to the computed VDE and adding the orbital energy differences relative to the HOMO.[45] In comparison of the simulated DOS spectra with the experimental spectra, the important part is how well the electron binding energies correspond to the spectral signature and not the relative intensities, so we only plotted out the stick DOS spectra, which are shown in Fig. S12 and S13 and the details are presented in Table S2 (ESI†). In order to better compare with the experimental spectra, we also simulated the DOS spectra of the selected isomers by fitting the computed VDEs with Gaussian functions of 0.20 eV full width at half maximum (FWHM). The simulated spectra together with the corresponding structures are presented in Fig. S14–S16 (ESI†). We labeled all isomers as n-a, n-b, ... where n stands for the number of water molecules. The structures that are similar to those in the reference of Asmis, Neumark and co-workers[20] are also labeled as n-I and n-II in each figure, and in this way it will be clear which are the new structures we found.

1. $HCO_3^-(H_2O)_n$ (n = 0–4). The bare HCO_3^- anion (C_s symmetry, $^1A'$ state) consists of one central carbon atom surrounded by three oxygen atoms in a trigonal planar arrangement, with a hydrogen atom attached to one of the oxygens. The symbols for the bond lengths (C–O bond: R_1, R_2, R_3, O–H bond: r) and bond angles (a_1, a_2, a_3) are all marked in Table S1 in the ESI.† The three C–O bond lengths are 1.23, 1.25, and 1.45 Å, respectively. The O–H bond length r is determined to be 0.96 Å. The bond angles for a_1, a_2, and a_3 are 132.76°, 113.34°, and 102.48°, respectively. All these values are obtained at the B3LYP/6-311++G** level and are consistent with those obtained at the higher level of theory MP2/aug-cc-pVTZ conducted by Wang and Xantheas.[10]

For $HCO_3^-(H_2O)_1$ clusters, the minimum energy isomer (labeled as 1-a, 1-I in ref. 20) has C_s symmetry in which the water forms two hydrogen-bonds with the negatively charged $-CO_2$ moiety of the HCO_3^- anion. The second isomer (1-b/1-II) also consists of doubly hydrogen-bonded water where the oxygen of the OH group and one O of the $-CO_2$ act as acceptors.

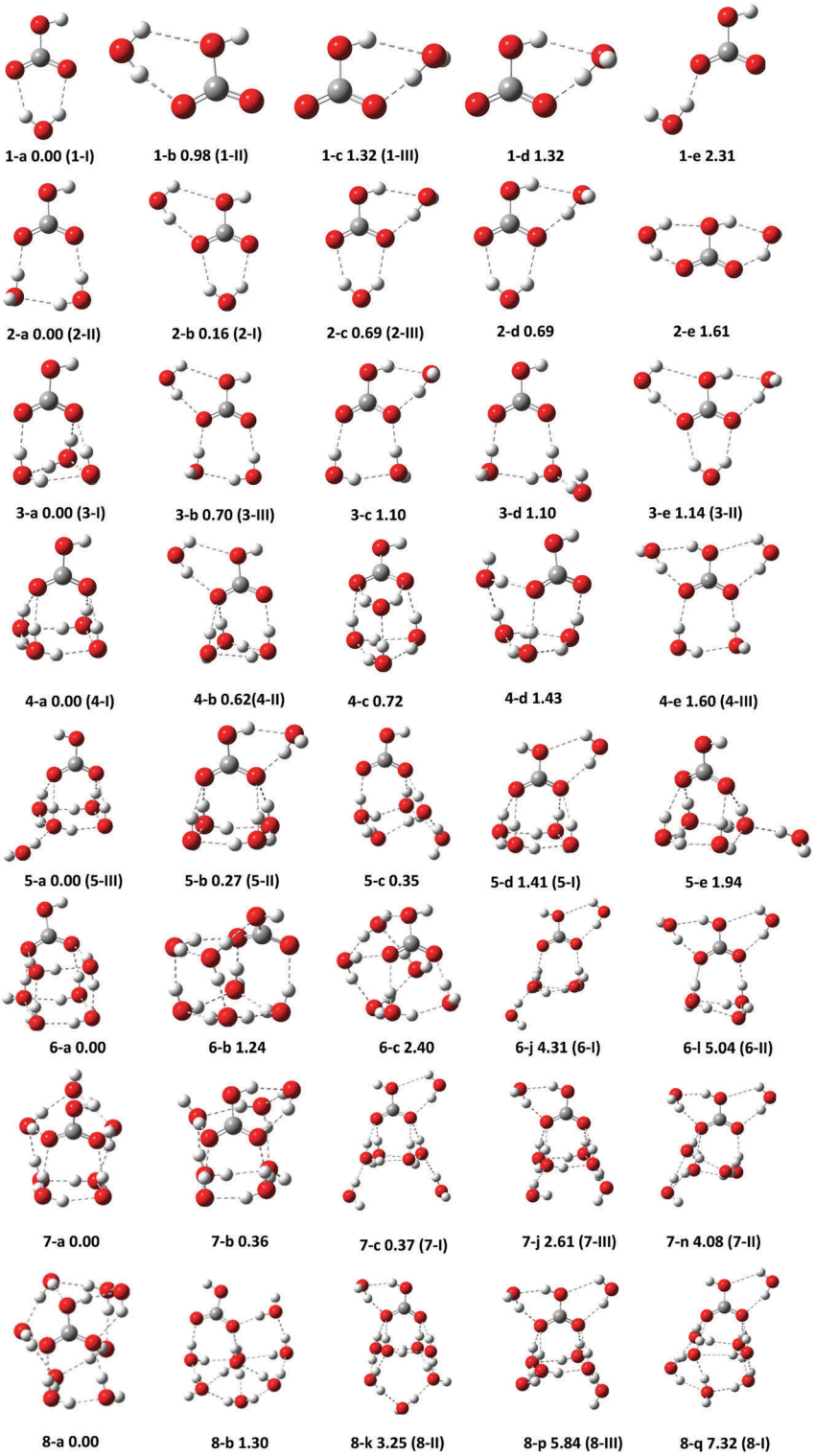

Fig. 3 Low-lying isomers of $HCO_3^-(H_2O)_n$ (n = 1–8) at B3LYP/6-311++G(3df,3pd) level of theory, relative energies (in kcal mol^{-1}) are indicated. The structures that are similar to those in ref. 20 are also labeled in parentheses.

This isomer is 0.98 kcal mol^{-1} higher in energy than 1-a. These results are in good agreement with what Asmis and co-workers found.[20] It should be noted that apart from the doubly hydrogen bonded isomers, one singly hydrogen bonded structure (1-e), which is 2.31 kcal mol^{-1} higher in energy has also been found. This is reminiscent of a recent infrared photodissociation spectroscopy and *ab initio* molecular dynamics simulations on $H_2PO_4^-(H_2O)$,[46] in which large amplitude motions over a small barrier involving the structures with the doubly and singly H-bonded water molecules were reported. The simulated

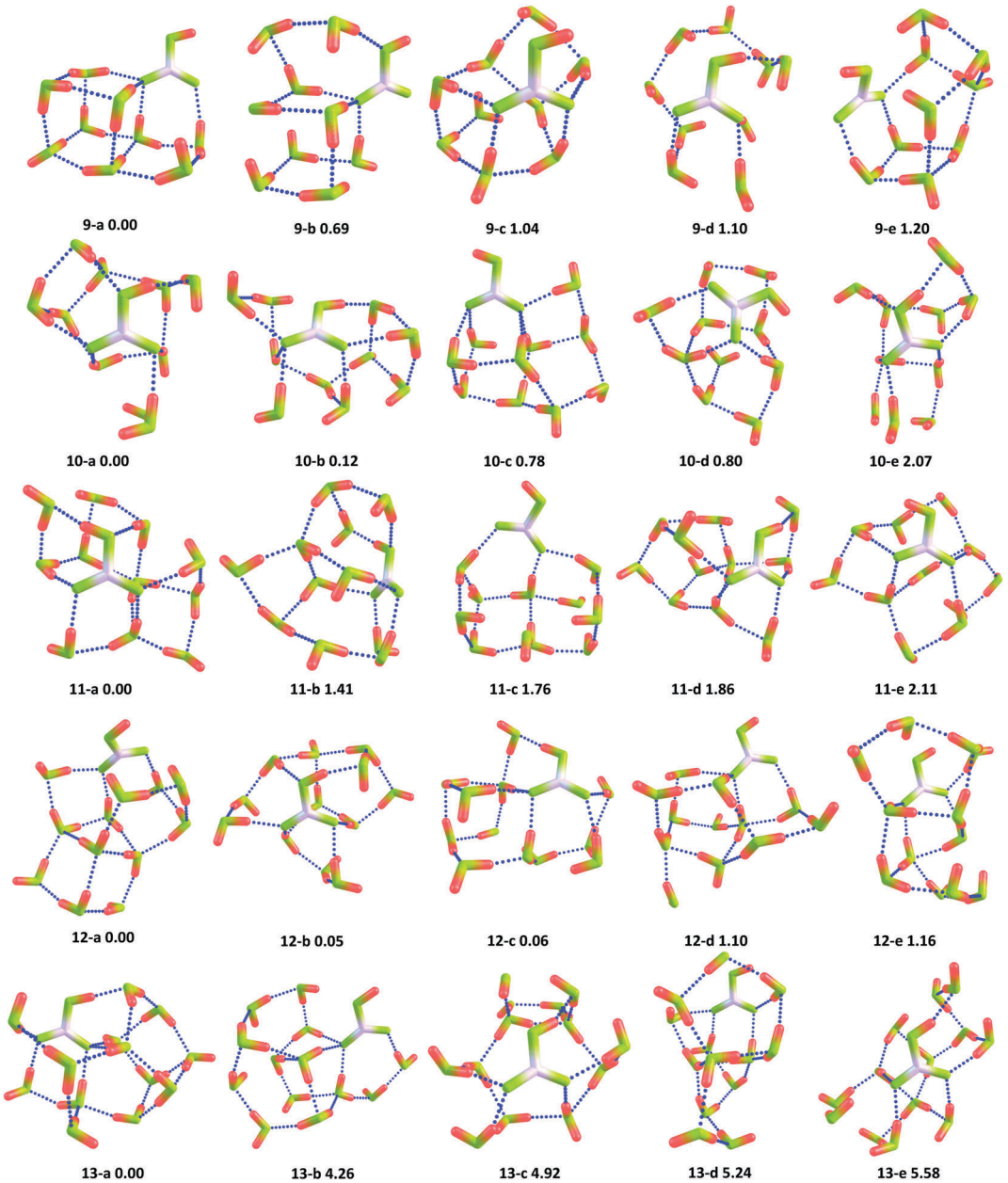

Fig. 4 Top five low-lying isomers of $HCO_3^-(H_2O)_n$ (n = 9–13) at B3LYP/6-311++G(3df,3pd) level of theory. Hydrogen bonds (blue dashed lines) less than 2 Å and the relative energies (in kcal mol^{-1}) are indicated. Red: H atom, green: O atom, light pink: C atom.

DOS spectra of $HCO_3^-(H_2O)_1$ are shown in Fig. S14 (ESI†), and the VDEs of isomers 1-a and 1-b calculated at the B3LYP/6-311++G(3df,3pd) level of theory are 4.84 and 4.80 eV, respectively, both agreeing with the experimental result of 4.85 eV pretty well. This suggests that they may both exist in the experiments.

The minimum energy isomer of the $HCO_3^-(H_2O)_2$ cluster (2-a/2-II) consists of two water molecules in the negatively charged $-CO_2$ moiety connected by a water–water hydrogen bond, each of which is singly bonded to the HCO_3^- core. Isomer 2-b, in which the water molecules are at different sites and each forms two H-bonds with HCO_3^-, is 0.16 kcal mol^{-1} higher in energy than 2-a. This isomer was found to be the minimum energy isomer (2-I) in ref. 20. Isomer 2-c (2-III) is 0.69 kcal mol^{-1} above isomer 2-a (2-II) and consists of two doubly hydrogen-bonded water molecules in two different positions of HCO_3^-. The simulated DOS spectra are also presented and the VDEs of the above mentioned isomers are 5.30, 5.46 and 5.25 eV, respectively. The VDE of the isomer 2-a (2-II) is much closer to the experimental value (5.35 eV) than other isomers.

For isomer 3-a (3-I) of the $HCO_3^-(H_2O)_3$ cluster, all three water molecules are in the negatively charged $-CO_2$ moiety, forming a cyclic water trimer, which forms three hydrogen bonds with the HCO_3^- anion. Isomer 3-b (3-III) in Fig. 3 has two water molecules in the negatively charged $-CO_2$ position and one in the COOH part, which is 0.70 kcal mol^{-1} higher

than isomer 3-a (3-I). The VDE of isomer 3-a (3-I) is 5.64 eV, in good agreement with the experimental value (5.70 eV). It should be noted that the isomer with three water molecules sitting at each of the three sites of HCO_3^-, 3-e (3-II) (Fig. 3), has also been obtained in this work. But it is 1.14 kcal mol^{-1} higher in energy than 3-a, and its calculated VDE value is 5.46 eV, 0.24 eV lower than the experimental value.

Fig. 3 and Fig. S2 (ESI†) show the results for the $HCO_3^-(H_2O)_4$ cluster. In the lowest energy isomer, all of the four water molecules are at the negatively charged $-CO_2$ part to form a water tetramer, in which each water forms one hydrogen-bond with the HCO_3^- anion, and another H-bond with an adjacent water molecule. The second isomer 4-b (4-II), lying 0.62 kcal mol^{-1} above the minimum energy isomer, has a water trimer, similar to isomer 3-a of the $HCO_3^-(H_2O)_3$ cluster, and a fourth water molecule in another position. The VDEs of isomers 4-a and 4-b are 6.02 and 5.96 eV, respectively, both close to the experimental value of 6.05 eV.

2. $HCO_3^-(H_2O)_n$ (n = 5–8). For the n = 5 cluster, the typical low-lying isomers are shown in Fig. 3 and Fig. S3 (ESI†). The two isomers 5-a and 5-d have a water tetramer hydrogen bonded to the negatively charged $-CO_2$ moiety, but the fifth water molecule is in a different position. In the lowest energy isomer, the fifth water molecule interacts with one water molecule of the water tetramer. It should be noted that we also found isomer 5-h with cubic structure formed by five water molecules and the HCO_3^- core, as shown in Fig. S3 (ESI†). This isomer is 3.80 kcal mol^{-1} above the lowest energy isomer at the B3LYP/6-311++G(3df,3pd) level of theory. However, this isomer was found to be the minimum energy isomer at the DF-LMP2 level of theory. The calculated VDEs are 6.19 (5-a/5-III), 5.86 (5-d/5-I), and 6.10 (5-h) eV, respectively. The VDE of isomer 5-a (5-III) is much closer to the experimental value of 6.30 eV.

In the lowest energy isomer of $HCO_3^-(H_2O)_6$, the six water molecules together with the two O atoms of the $-CO_2$ moiety form a cubic structure. Isomer 6-j (6-I), which can be developed from 5-a or 5-d and was identified as the most stable structure in the previous IR study,[20] lies 4.31 kcal mol^{-1} higher in energy than 6-a. Their calculated VDEs are 6.32 (6-a) and 6.40 eV (6-j), respectively. It can be seen that the calculated VDE of 6-j agrees a little better with the experimental value (6.50 eV).

For $HCO_3^-(H_2O)_7$, the structural motif of the most stable isomer changes a lot. It consists of a water pentamer and a water dimer, all forming hydrogen bonds with the HCO_3^- anion. Isomer 7-c (7-I) can be evolved from isomer 6-j (6-I), and it is 0.37 kcal mol^{-1} higher in energy than isomer 7-a. The calculated VDE of isomer 7-a is 6.40 eV, which is in agreement with the experimental value of 6.65 eV. However, the VDE of isomer 7-c is about 0.40 eV underestimated compared to the experimental value. Fig. 3 also shows five low-lying isomers of the $HCO_3^-(H_2O)_8$ cluster. Isomers 8-a and 8-q are structures both originating from the isomers 7-a and 7-c, respectively. The energy of isomer 8-q (8-I) is 7.32 kcal mol^{-1} higher than isomer 8-a. The calculated VDEs of these two isomers are pretty close to each other (6.51 and 6.46 eV, respectively), both agreeing with the experimental value of 6.75 eV.

3. $HCO_3^-(H_2O)_n$ (n = 9–13). Top five low-lying isomers of $HCO_3^-(H_2O)_{9-13}$ are presented in Fig. 4 in the 'stick' format in order to improve the structural visibility of those large clusters (the corresponding structures in the 'ball' format are given in the ESI†). The simulated PES spectra of two selected low-lying isomers of each large cluster, along with their structures and relative energies, are shown in Fig. S16 (ESI†). Those optimized structures do not show an obvious structural evolution path, and the configurations become more complicated as the cluster size increases. Most of the structures favor a water cube as the building unit. For the n = 9 cluster, the minimum energy isomer (9-a) is quite similar to that of $IO_3^-(H_2O)_n$ clusters recently studied;[47] which showed that the evolution of IO_3^- solvation proceeded in a cyclic fashion by building water tetramer layers, initially starting at the negatively charged oxygen side and eventually approaching contact with the cationic iodine side. Similarly, the $HCO_3^-(H_2O)_9$ cluster can be viewed as a previously formed water cubic hexamer simultaneously rotated out of the way to accommodate the addition of a water trimer. The calculated VDE of this isomer is 6.58 eV, about 0.27 eV underestimated compared with the experimental value (6.85 eV). As the water molecules increase (n = 10–13), the experimental VDEs no longer shift to the higher EBE region, which is roughly equal to 6.95 eV (Table 1). The calculated VDEs of the minimum energy isomers for n = 10–13 are 6.55, 6.61, 6.64, and 6.68 eV, respectively. All of them are underestimated by 0.4 to 0.3 eV compared with the experimental values. A similar amount of underestimation between the calculated VDEs and experimental ones was observed in the recent study of $IO_3^-(H_2O)_n$ clusters,[47] in which the same B3LYP functional was employed.

B. Discussion

1. Spectroscopic signatures and structural evolutions. From the NIPE spectra, we can see that the VDE incrementally increases with the cluster size from n = 1 to 10, and almost no further increases are seen for $n > 10$. It's quite difficult to identify the global minimum for each larger size hydrated $HCO_3^-(H_2O)_n$ cluster purely through the comparison between theoretical calculations and NIPES experiments alone, because the NIPE spectra shown in Fig. 1 are all broad and don't contain much structural hallmarks. In fact, we obtained a large number of isomers for each sized cluster, and their calculated VDEs are all within 0.5 eV compared with the experimental values. On the other hand, size-selected IR action spectroscopy represents a powerful method to study the ground state structures of hydrated clusters, as demonstrated by Asmis, Neumark and co-workers[20] in their recent work on the $HCO_3^-(H_2O)_{1-10}$ system. However, despite the fact that the size-selective IR spectra can provide rich structural signatures, it is still challenging in many cases to unequivocally identify the lowest energy isomers responsible for the observed IR spectra, particularly for large clusters, due to the possibility that different isomers may yield similar IR spectra. For example, we simulated the IR spectra of all isomers obtained for the monohydrated $HCO_3^-(H_2O)_1$ cluster, and found that the spectra from different isomers (including the singly hydrogen bond structure) are all

similar to the experimental one to some extent (Fig. S17, ESI†). Taking $HCO_3^-(H_2O)_4$ for instance, the previous IRMPD study showed that the simulated IR spectra of top two isomers (4-I and 4-II) were very similar, both in good agreement with the experimental spectrum; and both isomers were suggested to contribute to the observed spectrum.[20] Therefore there are slight uncertainties in identifying the lowest energy isomers that contributed to the observed spectra purely based on the comparison of experimental and simulated IR spectra as well. (More simulated IR spectra of $HCO_3^-(H_2O)_{2-4}$ and their comparison with the experimental spectra are presented in Fig. S18 (ESI†). We also simulated the IR spectra of the top isomers of $HCO_3^-(H_2O)_n$, n = 1–13 in the OH stretching region (2600–3900 cm^{-1}) at the B3LYP/6-311++G(3df,3d) level of theory, as shown in Fig. S22–S24 in the ESI,† to provide references for comparison with future IR work.) So here we propose a new research protocol by combining available IR spectra, NIPE spectra and unbiased structural searching methods, aiming to identify the lowest energy isomers of hydrated bicarbonate clusters. For the $HCO_3^-(H_2O)_4$ cluster, our study shows that the calculated VDE of isomer (4-a/4-I) (Fig. 3) agrees slightly better with the experimental value than isomer (4-b/4-II). Therefore, we can suggest isomer 4-a/4-I as the most probable structure observed in the experiments by combining the IR and NIPES results.

Fig. 5 displays our simulated IR spectra of the $HCO_3^-(H_2O)_n$ (n = 5–8) clusters. For $HCO_3^-(H_2O)_5$, both the simulated IR spectra of 5-a (5-III) and 5-d (5-I) are in reasonable agreement with the experiments. However, the calculated VDEs of isomers 5-a/5-III and 5-d/5-I are 6.19 and 5.86 eV, respectively; and the

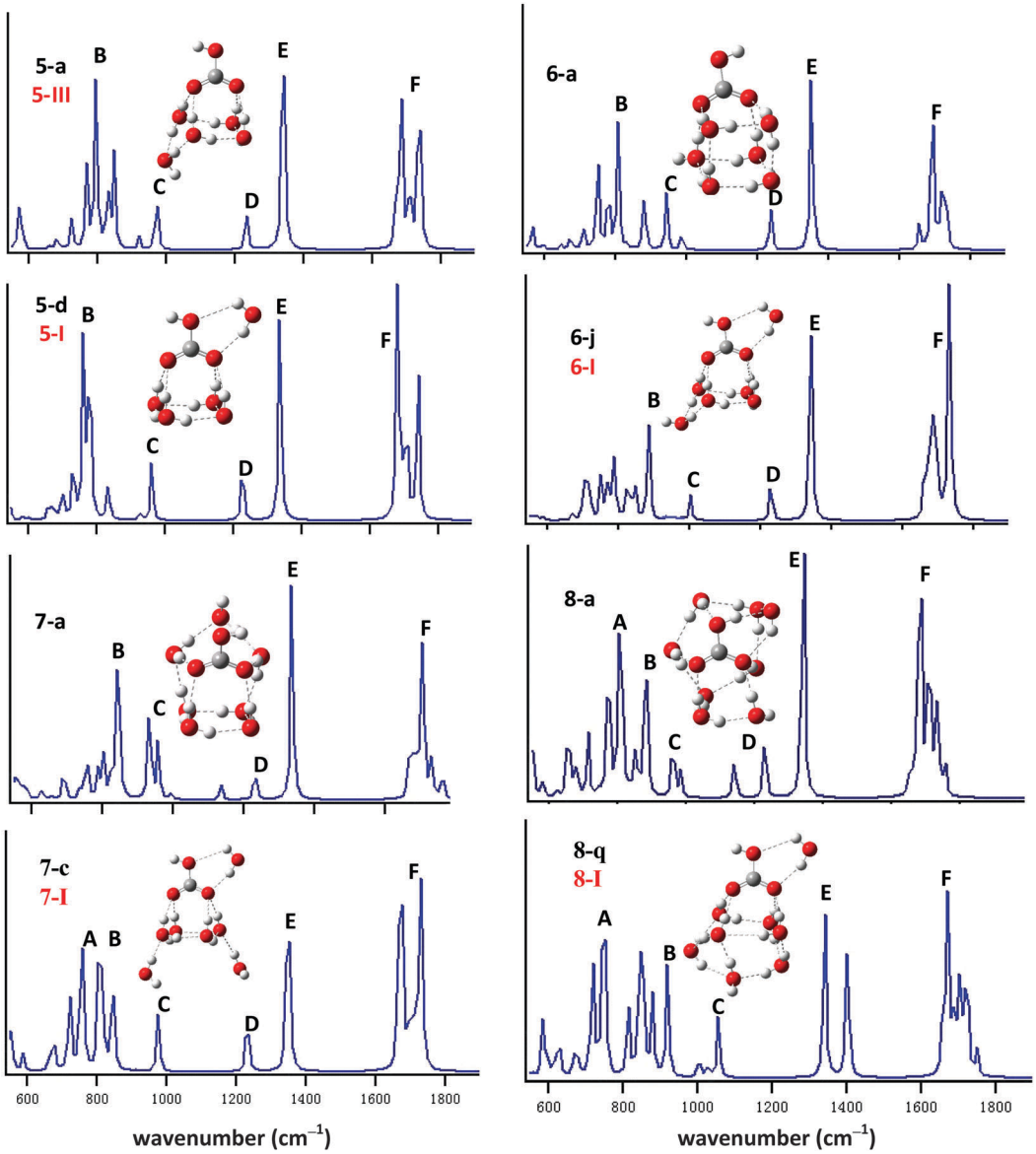

Fig. 5 Simulated IR spectra of $HCO_3^-(H_2O)_n$ (n = 5–8) with the structures of the low-lying isomers at the B3LYP/6-311++(3df,3pd) level of theory, marked n-a and n-b, respectively. The structures that are similar to those in ref. 20 are also labeled in red.

VDE of isomer 5-a (5-III) is much closer to the experimental result (6.30 eV). Hence, isomer 5-a (5-III) is proposed to be the best fit structure. It should be pointed out that by comparing the absorption peak position of the IR spectrum, the highly symmetric cubic shape isomer (5-h) (Fig. S19, ESI†) can be ruled out.

For $HCO_3^-(H_2O)_6$, the simulated IR spectra of the newly found isomer 6-a are presented in Fig. 5. Compared with isomer 6-j (6-I), the IR spectrum of 6-a showed one more peak between peaks B and C, which is inconsistent with the previous experimental report.[20] In addition, the latter one 6-j (6-I) seems to give a better calculated VDE (6.40 eV) compared to the experimental value of 6.50 eV than the former isomer 6-a (6.32 eV). Thus, we suspect that 6-j (6-I) is the main isomer detected in the experiments. For the $HCO_3^-(H_2O)_7$ cluster, our simulated IR spectrum based on the newly found isomer 7-a reproduces the experimental spectrum better around peaks C and D, and in particular, generates a weak peak between C and D, which was observed in the experimental spectrum,[20] but is missing in the simulated IR spectrum of isomer 7-c (7-I). Additionally, the calculated VDE of isomer 7-a is also closer to the experimental value (6.40 *vs.* 6.65 eV), while the VDE of isomer 7-c (7-I) is about 0.5 eV underestimated. Therefore, we suggest here that the newly obtained structure 7-a is the best fit structure for $HCO_3^-(H_2O)_7$.

The calculated VDEs of the two selected isomers (8-a and 8-q/8-I) are pretty close to each other (6.51 *vs.* 6.46 eV), both agreeing with the experimental value of 6.75 eV. We simulated the IR spectra of these isomers, and found that the simulated IR spectrum of isomer 8-a agrees better with the experimental IR spectrum between peaks C and E than that of 8-q (8-I). Thus, we propose that the newly found isomer 8-a is the best fit structure, likely to be the minimum energy structure of $HCO_3^-(H_2O)_8$.

The most probable structures detected in the experiments of $HCO_3^-(H_2O)_n$ (n = 1–8) clusters based on both the NIPE spectra and IR spectra are marked in red and presented in Fig. 6. For the even larger clusters, $HCO_3^-(H_2O)_n$ (n = 9–13), we cannot determine which isomer is the best fit structure due to the lack of the detailed IR spectra for n = 9, 10, and the fact that no IR spectra were obtained for n = 11–13 to be compared with. Thus, we chose the 'best fit structure' for each cluster (among the lowest energy isomers obtained at the B3LYP/6-311++G(3df,3pd) level of theory) based on the best agreement of its calculated VDE compared with the experimental VDE. The 'most probable structures' of each sized clusters are presented in Fig. S25 (ESI†). The comparison between their calculated VDEs and the experimentally measured VDEs/TDEs are plotted in Fig. 2, in which the respective trend is in good agreement with each other.

Three different evolutionary routes (distinguished in different colors) for the $HCO_3^-(H_2O)_n$ (n = 1–13) clusters are proposed in Fig. 6. Each route shows an obvious structural evolution in common from n = 1 to 4. Water molecules prefer to bind with

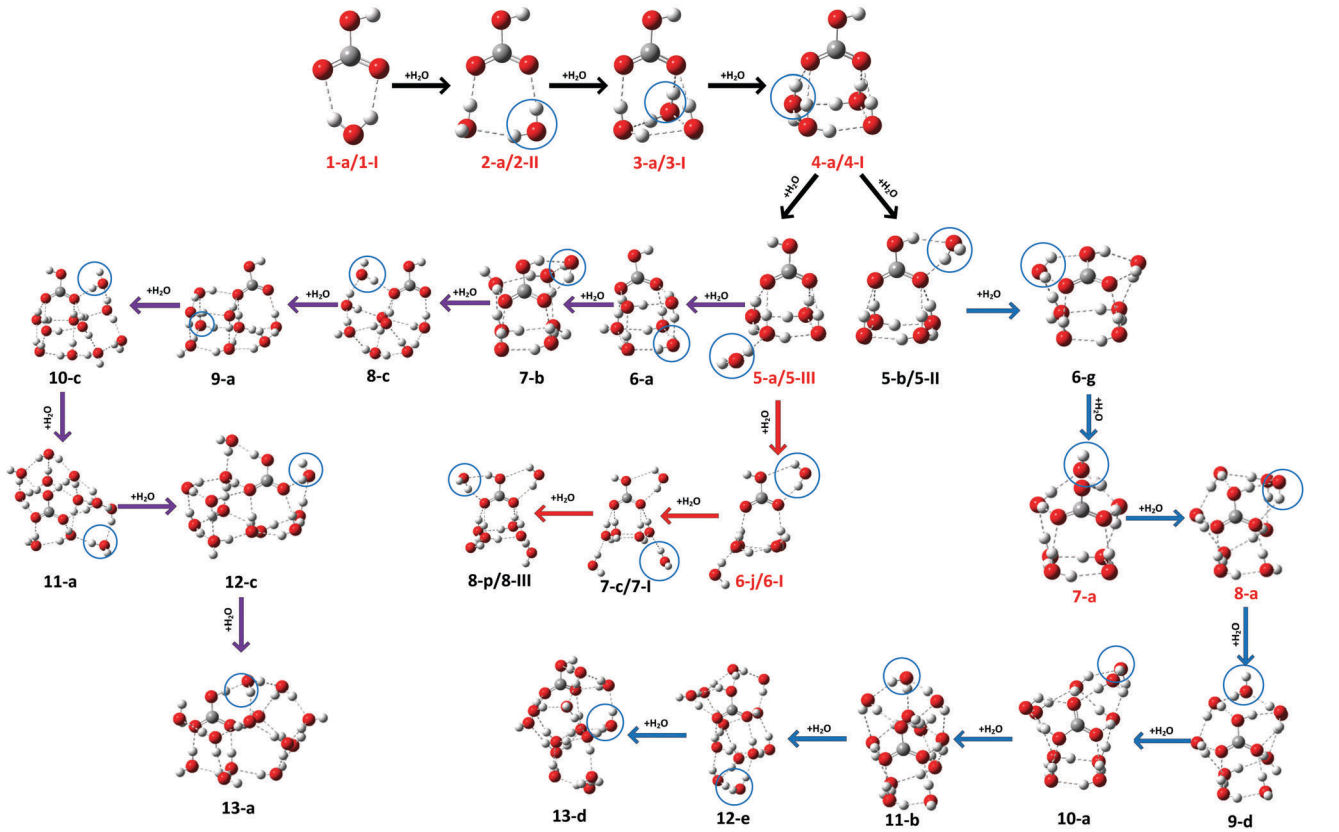

Fig. 6 Structural evolution of clusters from n = 1 to 13. Three different structural evolutionary paths (different colored arrows) are depicted. The inset blue rings indicate added water molecules. The isomers labeled in red are proposed to be the best fit structures.

the negatively charged $-CO_2$ moiety of the HCO_3^- anion, forming water dimer, trimer and tetramer configurations. The first route (red arrows) yields most of the structures obtained in the previous study,[20] and the building unit of the water tetramer is retained in all of the stable isomers of the clusters with n = 5–8. However, we did not find the relevant structures for larger clusters (n = 9–13) to be in accordance with this pathway. The second route (purple arrows) shows a water cubic structural transformation at n = 6. The structures following this route showed that the evolution of HCO_3^- solvation proceeds in a cyclic fashion by building water tetramer layers (*i.e.*, 6-a *versus* 9-a). As discussed above, most of structures along this pathway are those of lowest-energy within each size except 7-b, 8-c, 10-c, and 12-c. Thus, we inferred that 7-b and 8-c of relatively high energy may coexist in the experiments, and their simulated IR spectra are shown in Fig. S20 and S21 (ESI†). The simulated spectra are more or less in agreement with the experimental results. In the third route, the configuration transformed to the pentagon shape at n = 6, and the blue arrows showed the evolutionary process with the increasing water molecules in this route. In the experiments, these routes may coexist with different ratios. Each size cluster has a large number of isomers, especially for $n > 5$, in the different evolutionary processes. In principle, the growth of the cluster configuration can be viewed as a gradually increasing process. The lowest energy isomer of each size should have an embryo, which may result from an isomer of a smaller neighboring cluster; even this certain isomer may not be the lowest energy one. The participation of the higher energy isomers in the growth of the clusters may imply that different isomers with the same size could coexist with varying probabilities.

All of the results discussed above refer to the 0 K minimum energy structures. It should be mentioned that the previous study of $H_2PO_4^-(H_2O)$ showed that the assignments of the experimental IRMPD spectra based on the calculated harmonic frequencies and 0 K lowest energy isomer were not sufficient.[46] Considering large amplitude motions of water molecules and anharmonic effects resulted in much better agreement with the observed spectral signatures. This dynamic aspect of weakly bound clusters may be also important in bicarbonate–water clusters, and certainly warrants to be further explored in the future.

2. Charge distribution and molecular orbitals. The low-lying isomers of each cluster are shown in Fig. 3, 4 and Fig. S1–S11 (ESI†). Note that the general trend of HCO_3^- solvation is that for small clusters, water molecules prefer to bind with the $-CO_2^-$ negatively charged side (α side in ref. 20), in agreement with the previous study.[20] On the other hand, with the increase of water molecules, there is increasing evidence that water can bind with the –OH side (γ side). This may make sense because the acid dissociation constant (pK_a) of water is about 15, and the pK_a of HCO_3^- is 10.2, that means HCO_3^- is a weak acid and can auto-ionize in large water clusters to give proton and carbonate, which requires water molecules to solvate the –OH side of $HOCO_2^-$ in large clusters to initiate the deprotonation reaction.

From the experimental NIPE spectra, we suspect that the universal high EBE tails dominating in the large clusters are due to ionization of water. It is known that the threshold photoemission of liquid water occurs at 10.06 eV,[48] while the existence of a negative solute ion may make the ionization potential of water become lower, and lead to the observation of ionization of water in large hydrated clusters.[43] To explore this idea, we conducted the natural bond orbital (NBO) charge analyses. The NBO charges for the $HCO_3^-(H_2O)_n$ clusters are shown in Fig. 7 and Fig. S26–S30 (ESI†). The NBO charge analysis shows that the charge on HCO_3^- is about -0.965 e in $HCO_3^-(H_2O)_1$, while -0.903 e in $HCO_3^-(H_2O)_{10}$, indicating that with the increase of water molecules, there is gradual charge transfer from the solute HCO_3^- to the surrounding waters. This charge transfer will decrease the ionization potential of water. Furthermore, we also plotted out the frontier molecule orbitals (MOs) of $HCO_3^-(H_2O)_n$ for n = 1 and 10 in Fig. 7. It can be seen that for n = 1, the MOs are mainly contributed by the HCO_3^- anion core, while the HOMO-4 of the n = 10 cluster is mainly composed of contributions from water. In addition, the energy difference between the HOMO and HOMO−4 is relatively small (0.85 eV), consistent with the above argument that in the NIPE spectrum of $HCO_3^-(H_2O)_{10}$, the electron signal may mainly come from ionization of water.

3. Interaction nature. In order to study the bond interactions and the pair electron distributions of the $HCO_3^-(H_2O)_n$ clusters, we conducted the electron localization function (ELF) analysis using the Multiwfn 3.3.6 program package.[49] The color-filled ELF maps together with their contour lines of $HCO_3^-(H_2O)_1$ and $HCO_3^-(H_2O)_{10}$ clusters are presented in Fig. 8. The inset in the (1-a) plot shows the corresponding ELF map of the pure water molecule. Since the minimum structure of the $HCO_3^-(H_2O)_{10}$ cluster possesses a 3-dimensional configuration, two views along the (x,y) plane (plot 10-a) and the (C1–O2–H5) plane (plot 10-a′) are presented (the symbols of atoms are defined in Fig. S31, ESI†).

According to the ELF map, the blue area between the H_2O molecule and the HCO_3^- anion in $HCO_3^-(H_2O)_1$ implies weak interactions between the two molecules. The color on the H atoms shows red, which stands for a low probability of finding a second electron with the same spin in the neighboring region of the reference electron. It can be seen in Fig. 8 that the topological structures of ELF in the region of all C–O bonds are almost identical: the H atom of the water molecules is pointing toward the HCO_3^- anion, without being noticeably deformed. This implies that the HCO_3^-–water interactions are mainly of electrostatic nature. The hydrated HCO_3^- clusters are thus mainly bound by the dipole–charge electrostatic interactions. For the $HCO_3^-(H_2O)_{10}$ cluster, in the x–y plane, one oxygen atom of the bicarbonate core and four separated hydrogen atoms are clearly shown. All H atoms show a high value of ELF (in red color), indicating that the electrons are more likely confined in that region of space and may imply the existence of core electrons or lone pairs. In the 1(C)–2(O)–5(H) plane, a bicarbonate core and three adjacent water molecules are shown, where the values shown in the C atom and the three O atoms correspond to delocalized features. Similar electrostatic interactions are found for the $HCO_3^-(H_2O)_{10}$ cluster

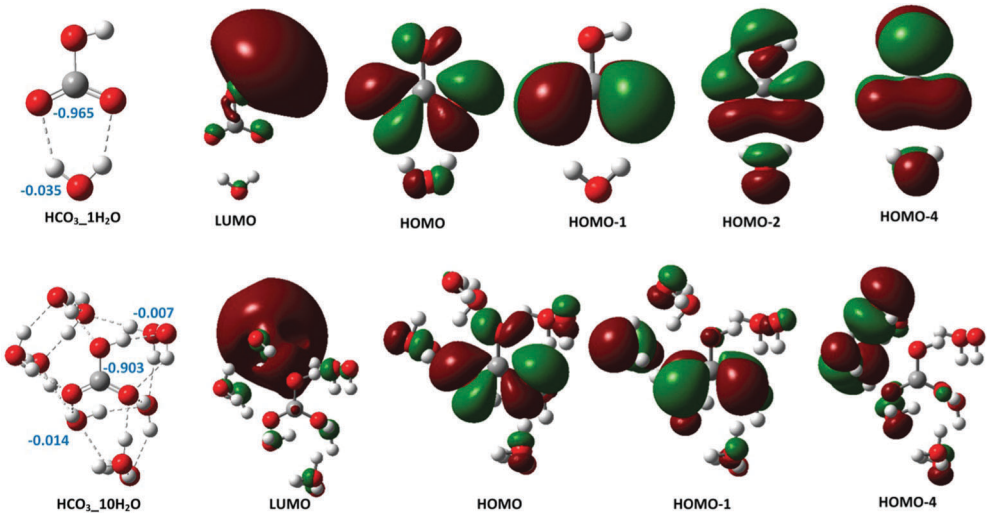

Fig. 7 Molecular orbitals of the minimum energy isomer of $HCO_3^-(H_2O)_1$ and $HCO_3^-(H_2O)_{10}$ clusters. The NBO charges on HCO_3^- and H_2O moieties are indicated in blue.

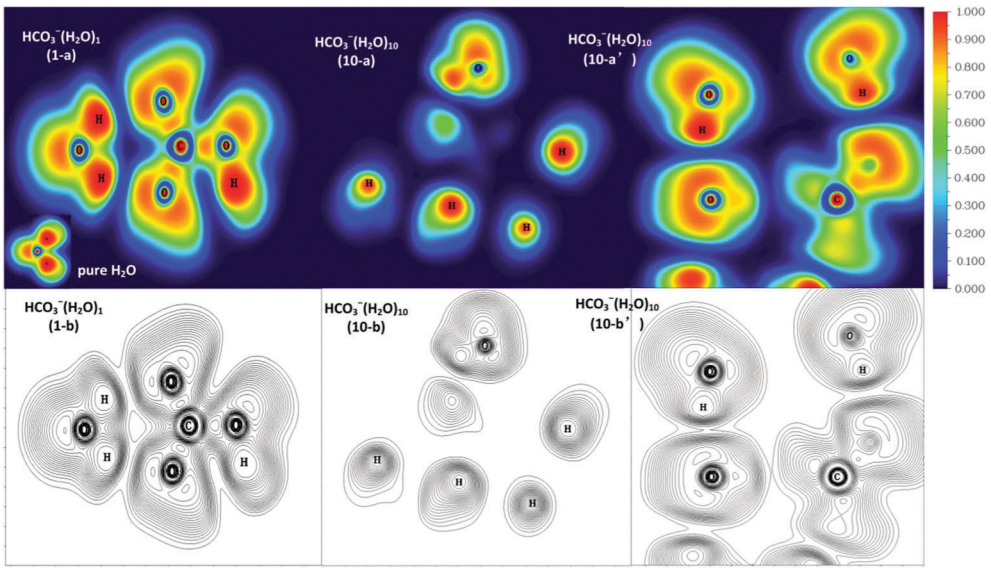

Fig. 8 The electron localization function (ELF) color-filled map (a) and the contour line map (b) of the $HCO_3^-(H_2O)_1$ and the $HCO_3^-(H_2O)_{10}$ clusters. The insert on the (1-a) is the ELF map of the pure water molecule. For the 3-dimensional structure of $HCO_3^-(H_2O)_{10}$ clusters, the 10-a and 10-a′ show the *x*,*y* plane and the 1 (C), 2 (O), 5 (H) plane (see Fig. S28 (ESI†) for definition of these three atoms), respectively. The color range is (0, 1). The value 0 corresponds to a delocalized system, and the value 1 corresponding to a completely localized region.

compared to that of $HCO_3^-(H_2O)_1$. In addition, the weak interaction between water molecules is also observed.

V. Conclusion

In conclusion, we investigated the $HCO_3^-(H_2O)_n$ (n = 0–13) clusters using NIPES and theoretical calculations. It was found that the EBEs of these clusters monotonically increase with the cluster size up to n = 10, while the spectra no longer shift to the high EBE region after n > 10. Besides, the photoelectron spectral feature from the photo-detachment of HCO_3^- itself diminishes with the increase of water coverage. By comparing the theoretical VDEs, the simulated NIPE spectra with the experimental spectra, and by comparing the simulated IR spectra with the IRMPD experimental results of Asmis and co-workers, we obtained the most probable structures for each size cluster, explored their structural evolution, and proposed three cluster growth routes. At a smaller size, water tends to interact with the charged end of $-COO^-$ due to the dominant charge–dipole interaction. As the cluster size increases, the negative charge of the solute is gradually screened, while water–water and $(O_2)COH$–water hydrogen bonding interactions become comparable to the charge–dipole interaction, giving rise

to a plethora of low energy isomers. It is interesting to note that the solute of HCO_3^- is always at the exterior of the hydrated clusters, suggesting that bicarbonate is a weakly hydrated anion with comparable solute–solvent and solvent–solvent interactions.

Although both the IR and NIPE spectra could provide abundant structural and energetic information, it is still quite challenging to identify the global minima purely relied on only one single method. This work demonstrates the feasibility of combining NIPES, IRMPD as well as theoretical calculations in determining the minimum energy isomers that best fit the experiments. From the NBO charge distributions and molecular orbitals analyses, the universal high EBE tails that dominate in the large clusters can be ascribed to the ionization of solvent water, confirming the experimental observations. In addition, ELF analysis reveals that the bicarbonate–water interactions are mainly of electrostatic nature.

Acknowledgements

The experimental work done at PNNL was supported by the U. S. Department of Energy (DOE), Office of Science, Office of Basic Energy Sciences, the Division of Chemical Sciences, Geosciences, and Biosciences, and was performed using EMSL, a national scientific user facility sponsored by DOE's Office of Biological and Environmental Research and located at Pacific Northwest National Laboratory, which is operated by the Battelle Memorial Institute for the DOE. The theoretical work was supported by the National Natural Science Foundation of China (Grant No. 21403244, 21573241 and 41527808), the State Key Program of National Natural Science of China (Grant No. 21133008), the National High Technology Research and Development Program of China (863 Program No. 2014AA06A501) and the "Interdisciplinary and Cooperative Team" of CAS. Acknowledgement is also made to the "Thousand Youth Talents Plan". Part of the computation was performed by Cascade in EMSL, and part of the computation was performed at the Supercomputing Center of the CAS and Supercomputing Center of USTC.

References

1 K. Caldeira and M. E. Wickett, *Nature*, 2003, **425**, 365.
2 J. M. C. Plane, *Ann. Geophys.-Atmos. Hydrospheres Space Sci.*, 2000, **18**, 807–814.
3 A. Tongraar, P. Yotmanee and A. Payaka, *Phys. Chem. Chem. Phys.*, 2011, **13**, 16851–16860.
4 D. N. Silverman and S. H. Vincent, *Crit. Rev. Biochem.*, 1983, **14**, 207–255.
5 D. N. Silverman and S. Lindskog, *Acc. Chem. Res.*, 1988, **21**, 30–36.
6 I. Kurtz, D. Petrasek and S. Tatishchev, *J. Membr. Biol.*, 2004, **197**, 77–90.
7 B. D. Sharma, *Acta Crystallogr.*, 1965, **18**, 818–824.
8 R. R. Squires, *Int. J. Mass Spectrom. Ion Processes*, 1992, **117**, 565–600.
9 P. M. Hierl and J. F. Paulson, *J. Chem. Phys.*, 1984, **80**, 4890–4900.
10 X.-B. Wang and S. S. Xantheas, *J. Phys. Chem. Lett.*, 2011, **2**, 1204–1210.
11 Z. Peng and K. M. Merz, *J. Am. Chem. Soc.*, 1993, **115**, 9640–9647.
12 M. M. Davidson, I. H. Hillier, R. J. Hall and N. A. Burton, *Mol. Phys.*, 1994, **83**, 327–333.
13 A. V. Nemukhin, I. A. Topol, B. L. Grigorenko and S. K. Burt, *J. Phys. Chem. B*, 2002, **106**, 1734–1740.
14 K. Iida, D. Yokogawa, H. Sato and S. Sakaki, *Chem. Phys. Lett.*, 2007, **443**, 264–268.
15 K. Leung, I. M. B. Nielsen and I. Kurtz, *J. Phys. Chem. B*, 2007, **111**, 4453–4459.
16 P. P. Kumar, A. G. Kalinichev and R. J. Kirkpatrick, *J. Phys. Chem. B*, 2009, **113**, 794–802.
17 R. G. Keesee, N. Lee and A. W. Castleman, *J. Am. Chem. Soc.*, 1979, **101**, 2599–2604.
18 W. W. Rudolph, D. Fischer and G. Irmer, *Appl. Spectrosc.*, 2006, **60**, 130–144.
19 W. W. Rudolph, G. Irmer and E. Koenigsberger, *Dalton Trans.*, 2008, 900–908.
20 E. Garand, T. Wende, D. J. Goebbert, R. Bergmann, G. Meijer, D. M. Neumark and K. R. Asmis, *J. Am. Chem. Soc.*, 2010, **132**, 849–856.
21 V. Vchirawongkwin, A. B. Pribil and B. M. Rode, *J. Comput. Chem.*, 2010, **31**, 249–257.
22 X.-B. Wang and L.-S. Wang, *Rev. Sci. Instrum.*, 2008, **79**, 073108.
23 M. Z. Kamrath, E. Garand, P. A. Jordan, C. M. Leavitt, A. B. Wolk, M. J. Van Stipdonk, S. J. Miller and M. A. Johnson, *J. Am. Chem. Soc.*, 2011, **133**, 6440–6448.
24 X.-B. Wang, Y.-L. Wang, J. Yang, X.-P. Xing, J. Li and L.-S. Wang, *J. Am. Chem. Soc.*, 2009, **131**, 16368–16370.
25 D. J. Goebbert, T. Wende, R. Bergmann, G. Meijer and K. R. Asmis, *J. Phys. Chem. A*, 2009, **113**, 5874–5880.
26 X.-B. Wang, X.-P. Xing and L.-S. Wang, *J. Phys. Chem. A*, 2008, **112**, 13271–13274.
27 D. J. Wales and J. P. K. Doye, *J. Phys. Chem. A*, 1997, **101**, 5111–5116.
28 H. Wen, Y.-R. Liu, T. Huang, K.-M. Xu, W.-J. Zhang, W. Huang and L.-S. Wang, *J. Chem. Phys.*, 2013, **138**, 174303.
29 K.-M. Xu, T. Huang, H. Wen, Y.-R. Liu, Y.-B. Gai, W.-J. Zhang and W. Huang, *RSC Adv.*, 2013, **3**, 24492–24502.
30 L.-L. Yan, Y.-R. Liu, T. Huang, S. Jiang, H. Wen, Y.-B. Gai, W.-J. Zhang and W. Huang, *J. Chem. Phys.*, 2013, **139**, 244312.
31 H. Wen, Y.-R. Liu, K.-M. Xu, T. Huang, C.-J. Hu, W.-J. Zhang and W. Huang, *RSC Adv.*, 2014, **4**, 15066–15076.
32 Y.-R. Liu, H. Wen, T. Huang, X.-X. Lin, Y.-B. Gai, C.-J. Hu, W.-J. Zhang and W. Huang, *J. Phys. Chem. A*, 2014, **118**, 508–516.
33 J. P. Perdew, K. Burke and M. Ernzerhof, *Phys. Rev. Lett.*, 1996, **77**, 3865–3868.
34 B. Delley, *J. Chem. Phys.*, 1990, **92**, 508–517.

35 K. Raghavachari and G. W. Trucks, *J. Chem. Phys.*, 1989, **91**, 1062–1065.
36 A. J. Cohen and N. C. Handy, *Mol. Phys.*, 2001, **99**, 607–615.
37 X. Xu and W. A. Goddard, *Proc. Natl. Acad. Sci. U. S. A.*, 2004, **101**, 2673–2677.
38 Y. Zhao and D. G. Truhlar, *Theor. Chem. Acc.*, 2008, **120**, 215–241.
39 J. P. Perdew, K. Burke and Y. Wang, *Phys. Rev. B: Condens. Matter Mater. Phys.*, 1996, **54**, 16533–16539.
40 M. J. Frisch, H. B. Schlegel, G. E. Scuseria, M. A. Robb, G. Scalmani, V. Barone, B. Mennucci, A. Petersson, M. Caricato, X. Li, H. P. Hratchian, J. B. A. F. Izmaylov, G. Zheng, J. L. Sonnenberg and M. Hada, *et al.*, *Gaussian 09, Revision A.02*, Gaussian, Inc., Wallingford, CT, 2009.
41 H.-J. Werner, P. J. Knowles, G. Knizia, F. R. Manby and M. Schuetz, *Wiley Interdiscip. Rev.: Comput. Mol. Sci.*, 2012, **2**, 242–253.
42 P. J. K. H. J. Werner, G. Knizia, F. R. Manby and M. Schuetz, *Molpro, version 2010.1, a package of ab initio program*, 2010.
43 X. B. Wang, X. Yang, J. B. Nicholas and L. S. Wang, *Science*, 2001, **294**, 1322–1325.
44 D. J. Tozer and N. C. Handy, *J. Chem. Phys.*, 1998, **109**, 10180–10189.
45 H. Hakkinen, B. Yoon, U. Landman, X. Li, H. J. Zhai and L. S. Wang, *J. Phys. Chem. A*, 2003, **107**, 6168–6175.
46 L. Jiang, S. T. Sun, N. Heine, J. W. Liu, T. Yacovitch, T. I. Wende, Z. F. Liu, D. M. Neumark and K. R. Asmis, *Phys. Chem. Chem. Phys.*, 2014, **16**, 1314–1318.
47 H. Wen, G.-L. Hou, S. M. Kathmann, M. Valiev and X.-B. Wang, *J. Chem. Phys.*, 2013, **138**, 031101.
48 J. V. Coe, A. D. Earhart, M. H. Cohen, G. J. Hoffman, H. W. Sarkas and K. H. Bowen, *J. Chem. Phys.*, 1997, **107**, 6023–6031.
49 T. Lu and F. Chen, *J. Comput. Chem.*, 2012, **33**, 580–592.

